

# Dissipative-regime measurements as a tool for confirming and characterizing near-room-temperature superconductivity

Charles L. Dean and Milind N. Kunchur\*

*Department of Physics and Astronomy, University of South Carolina, Columbia, SC 29208*

The search for new superconducting materials approaching room temperature benefits from having a variety of testing methodologies to confirm and characterize the presence of superconductivity. Often the first signatures of new superconducting species occur incompletely and in very small volume fractions. These trace amounts may be too weak to produce an observable Meissner effect and the resistance may not go completely to zero if the percolation threshold is not met. Under these conditions, secondary behavior—such as transitions or cross overs in the temperature dependence of magnetoresistance, magnetic irreversibility, or thermopower—are often used as indications for the presence of superconductivity. Our group has developed a rather unique set of fast-timescale and dissipative transport measurements that can provide another tool set for confirming and characterizing suspected superconductivity. Here we provide some background for these methods and elucidate their collaborative value in the search for new superconducting materials.

Keywords: pairbreaking, pair-breaking, vortex, vortices, theory, tutorial, RTS, room-temperature superconductivity, superconductor, detection, characterization

PACS numbers:

Keywords:

## INTRODUCTION

The recent observation of 203 K superconductivity in  $\text{H}_3\text{S}$  [1] under pressure and possible hints of superconductivity above room temperature in graphite [2] have once again fired up interest and hope in the detection and synthesis of materials that superconduct at and above room temperatures. The potential technological impact and scientific importance of the realization of room-temperature superconductivity needs no further explanation or emphasis. The initial detection of a new superconducting species often occurs in trace amounts in inhomogeneous samples. In such cases, the classic abrupt resistance drop to zero and the appearance of clear cut Meissner flux expulsion may be luxuries that cannot be had. Even in the case of homogeneous samples that do show the above signatures, there remains the further issue of characterizing the superconducting parameters. The mixed-state upper critical field  $B_{c2}$ , reflective of the coherence length  $\xi$ , and the penetration depth  $\lambda$ , reflective of the superfluid density  $\rho_s=1/\lambda^2$ , are two crucial measurements that are amongst the first to be performed. There are multiple techniques for determining such parameters, each of which has its own advantages and limitations. Our group has developed some uncommon—and in some cases unique—experimental techniques that investigate superconductors at ultra-short time scales, and under unprecedented and extreme conditions of current density  $j$ , electric fields  $E$ , and power density  $p = \rho j^2$  (where  $\rho$  is the resistivity). These techniques have led to the discovery or confirmation of several novel phenomena and regimes in superconductors, and in addition provide an alternative method to glean information on fundamental superconducting parameters, which in some cases may

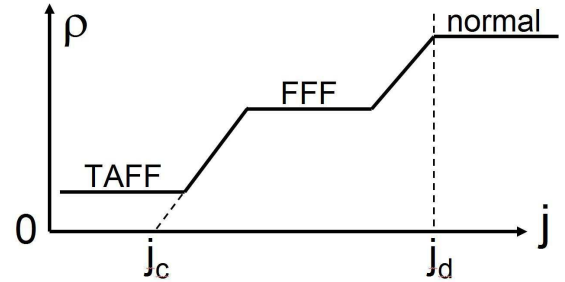


FIG. 1: Progression of stages of dissipation, which alternate between Ohmic ( $R=\text{const}$ ) and non-linear regimes.

be hard to obtain by other methods. These techniques therefore bear a special relevance in collaborative work that involves the search for new superconducting materials.

## BACKGROUND

In the discussion that follows, it will be assumed that the superconductor is of type II and enters the mixed state with quantized magnetic flux vortices above a lower critical magnetic field  $B_{c1}$ . As the transport current density  $j$  in a superconductor is steadily increased, the behavior of the superconductor goes through a progression of stages [3] as illustrated in Fig. 1. If not in the Meissner state and if vortices are present, there is initially some finite resistance because of flux motion. In the limit of very low driving forces, this regime can be Ohmic ( $R=\text{const}$ ) and can be described by process such as TAFF (thermally activated flux flow) or variations thereof. As  $j$  is increased, there is a non-linear response as vortices get

depinned and commence to move more easily leading to increasing resistivity. At some point the vortices become completely depinned and flow freely. Under this condition, the resistivity stops increasing and there is an intermediate plateau of constant  $\rho = \rho_f$ . The resistivity  $\rho_f$  in this free-flux-flow (FFF) state bears a relatively simple relationship, often referred to as the Bardeen-Stephen equation, to the normal-state resistivity  $\rho_n$  and the applied  $B$ :

$$\rho_f \sim \rho_n B / B_{c2} \quad (1)$$

This relationship at once ties the measurable quantity  $\rho_f$  to  $\rho_n$  and  $B_{c2}$ . An understanding of the normal state—the nature of the charge carriers, their concentration, and their scattering rates—is an important step in developing an understanding of the superconducting state. Therefore a knowledge of  $\rho$  over the entire temperature range, including well below  $T_c$ , provides an important step in elucidating the normal state. If  $B_{c2}$  is known, Eq. 1 provides  $\rho_n$ ; on the other hand if  $\rho_n$  is known, Eq. 1 provides  $B_{c2}$  (which may be impossible to reach at  $T \ll T_c$  because of possibly prohibitively high values). Flux flow thus provides a window to the normal state and upper critical field well below  $T_c$  without the need to suppress the superconducting state through very high magnetic fields  $B_{c2}(T \ll T_c)$ . The main obstacle to this approach is that unless one is in a free-flux-flow state, presence of pinning alters Eq. 1 in potentially complicated ways making it less reliable to relate the observed  $\rho$  to basic parameters. Overcoming pinning requires applying a Lorentz driving force  $\vec{F}_L = d(j \times \vec{\Phi}_0)$  (where  $d$  is the thickness) that well exceeds the pinning force  $F_p$ . The current density required for this is often of such a high value, that the superconductor becomes intensely dissipative. As an example, in optimally pinned  $\text{Y}_1\text{Ba}_2\text{Cu}_3\text{O}_7$  (where the conventional critical current density  $j_c$  approaches the pair-breaking value  $j_d$ ), one needs a  $j \sim j_d > 10^8$  A/cm<sup>2</sup> at low temperatures. Given that  $\rho_n \sim 100$   $\mu\Omega\text{-cm}$  for  $\text{Y}_1\text{Ba}_2\text{Cu}_3\text{O}_7$ , this entails a power dissipation density of  $p = \rho j^2 > 10^{12}$  W/cm<sup>3</sup>. This is of course a worst-case scenario, and the majority of superconducting systems will not have such a combination of simultaneously high  $\rho_n$  and  $j_c$  (ultra high pinning); however, it is common for the dissipation densities to get above  $10^8$  W/cm<sup>3</sup>, which can cause an objectionable temperature rise, if not sample destruction, if a continuous excitation is used for the transport  $IV$  curve. The experimental confirmation of the Bardeen-Stephen law of Eq. 1, was in fact one of the motivations for us to develop the pulsed-signal techniques (described in the Methods section below) which can achieve low duty cycles of  $< 1$  ppm and low effective sample thermal resistances of  $< 1$  nK-cm<sup>3</sup>/W, and permit measurements at  $p \sim 10^{10}$  W/cm<sup>3</sup>.

When  $j$  is increased beyond the central free-flux-flow plateau of Fig. 1, the response once again becomes non-linear and  $R$  rises as the pair breaking action of the

current suppresses the superconductivity until it is completely quenched and the system enters the normal state when  $j$  reaches its depairing (pair-breaking) value  $j_d$ . Here, once again,  $R = \text{const.}$  (If  $B=0$ , the first three distinct stages will be absent and  $R$  will rise non-linearly from zero directly to  $\rho_n$ .) This  $j_d$  is a measure of the superfluid density  $\rho_s \equiv 1/\lambda^2$  through the relation [4]:

$$j_d(0) = \sqrt{\frac{8\Phi_0 B_{c2}(0)}{27\mu_0^3 \lambda^4(0)}} \quad (2)$$

Eq. 2 provides a way to estimate  $\lambda$  and hence  $\rho_s$  through purely transport measurements (as  $B_{c2}$  can also be measured through a transport measurement). This is especially useful when the quantity of the superconducting material is too small and/or the geometry is unsuitable for susceptibility and inductive type of measurements. Current induced pair breaking also provides another secondary detection of superconductivity. Just as a magnetic field shifts a superconducting transition downward in  $T$ , the transition shifts downward with increasing  $j$ . This current induced shift follows a  $\Delta T_c \propto j^{2/3}$  behavior. This two-third power law can be used as another confirmation/indication that a resistive drop is due to superconductivity and not some other effect. Like the Meissner effect,  $j_d$  goes to the heart of the superconducting state through the distinctive way in which a current suppresses  $\rho_s$ . As with the observation of FFF, observing current induced pair breaking requires current densities of the highest magnitude that the superconductor can support. Near the transition,  $j_d$  has a smaller value (vanishing as  $T \rightarrow T_c$ ); however, the system is especially sensitive to small changes in  $T$  that might result from macroscopic Joule heating. Hence this investigation also needs very short low-duty-cycle signals. The next section describes the experimental set up for conducting experiments with high pulsed current densities, and the section that follows summarizes the novel results that have come out of such investigations and how they pertain to the detection and characterization of new near-room-temperature superconducting materials.

## EXPERIMENTAL METHODS

### Electrical measurements

Our transport studies in superconductors include ac, continuous-dc, and pulsed signals. However the most distinguishing capability of our group is its expertise in developing techniques and specialized measurements using pulsed signals. Fast ( $>100$  GHz sampling rate) digital-storage oscilloscopes (DSO) in conjunction with in-house built pulsed sources and detection electronics are used for this purpose. The specific electronics is customized for every experiment.

There are two types of pulsed measurements. The first type is a quasi-dc measurement, shown in Fig. 2, in which  $I(t)$  and  $V(t)$  are measured on the flat top portions of the pulses corresponding to the zero-frequency limit. The sole purpose of this pulsing is to reduce the duty cycle ( $\sim 1$  ppm) and consequent Joule heating, leading to effective thermal resistances  $R_{th} = \Delta T/dp$  in the  $1 \text{ nK}-1 \mu\text{K}\cdot\text{cm}^3/\text{W}$  range. Pulsing also makes heating at contacts irrelevant because the thermal diffusion distance,  $\sqrt{D\tau} \sim 9-84 \mu\text{m}$ , is shorter than the contacts-to-bridge distance (few mm).

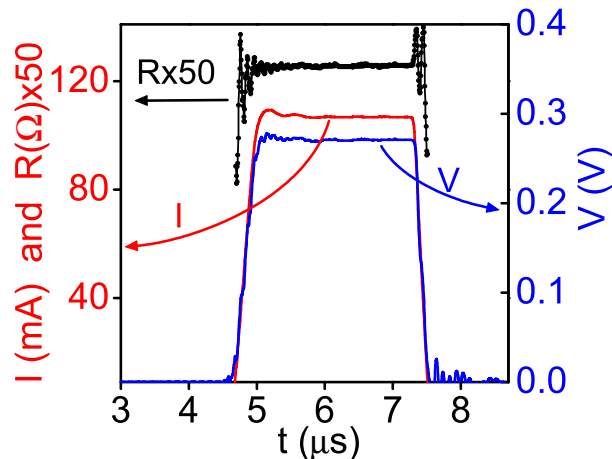


FIG. 2: Some typical quasi-dc high-dissipation pulse waveforms.  $j = 9.7 \text{ MA}/\text{cm}^2$ ,  $E = 83 \text{ V}/\text{cm}$ , and  $p = jE = 803 \text{ MW}/\text{cm}^3$  on the plateaus. (Adapted from Topical Review by M. N. Kunchur, J. Phys.: Condens. Matter **16**, R1183.)

The other type of pulsed measurement explicitly probes the time dependence of  $I(t)$  and  $V(t)$  and cross correlates them with sub-nanosecond accuracy. These measurements required significant developments in the sensing circuits for simultaneously  $I(t)$  and  $V(t)$  measurements, and in the preamplifiers and pulsed sources. Also an “artificial ground” approach was developed to better isolate the small signals in the voltage leads from the huge fast varying signals in the current leads. Fig. 3 shows the performance of this system under resistive and inductive loads. An important distinction of this apparatus is that this is not simply an impulse measurement. In measurements employing laser pulses or ultrashort current pulses generated by Josephson electronics, the stimulus is not monitored at all during the measurement and only the response is monitored. In our setup, both  $I(t)$  and  $V(t)$  are simultaneously monitored with high accuracy and can be correlated instant for instant in the time domain. That makes this technique unique and opens the doors for correlated  $I(t)-V(t)$  investigations of other phenomena in condensed-matter systems.

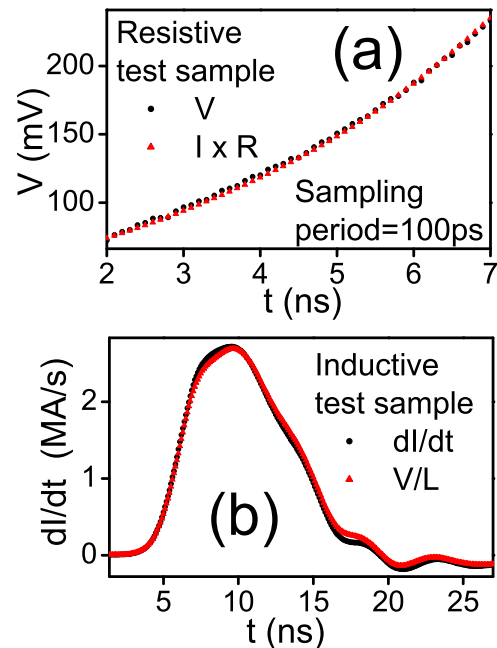


FIG. 3: (a)  $V(t)$  and  $I(t) \times R$  for a test resistor and in place of a superconducting sample. (b)  $dI/dt$  and  $V(t)/L$  for a test inductor in place of a superconducting sample. The voltages across the purely resistive or inductive loads are seen to track their respective current or current-derivative functions with subnanosecond accuracy. (Adapted from G. F. Saracila and M. N. Kunchur, Phys. Rev. Lett. **102**, 077001.)

Further information regarding the instrumentation and other experimental details can be found in two review articles [4, 5].

### Cryogenics

The cryostats and magnetic field environments used in our work consist of liquid-helium based as well as closed-cycle systems: (1) An Oxford Instruments 16-Tesla superconducting magnet with  $\text{He}^4$  and  $\text{He}^3$  cryostats ( $0.28 < T < 310 \text{ K}$ ). (2) A highly customized Cryomech pulsed-tube cryocooler ( $2.8 < T < 350 \text{ K}$ ) with a 1.2 T rotating water-cooled magnet (an advanced triggering method employing acoustic feedback provides extremely stable temperatures for long durations). (3) A single-stage ( $30 < T < 375 \text{ K}$ ) Cryomech pulsed-tube cryocooler that has a very large sample space ( $\sim 150 \text{ cm}^3$ ) and would be especially suitable for measurements on superconducting samples maintained in high-pressure cells. (4) And a Quantum Design PPMS with a custom insert developed for conducting short-timescale measurements (In order to greatly reduce noise, the sample environment and shields of wires within this apparatus are connected to a special highly effective ground consisting of a large loop of 3/4" diameter copper wire buried deep under-

ground.

## PHENOMENA AND REGIMES THAT CAN BE STUDIED

Our wide-spectrum pulsed-transport measurements enter uncharted space and push various parameters to unprecedented extremes (e.g.,  $E > 1000$  V/cm,  $p = jE > 10^{10}$  W/cm<sup>3</sup>, and vortex velocity  $v_\phi > 10$  km/s). Thus a rich variety of physics is uncovered and valuable new information is obtained about fundamental parameters. Below we give just a few examples of the types phenomena and regimes that we can study with our techniques.

### Ballistic superfluid acceleration and superfluid density suppression

One of the most direct ways for measuring superfluid density is through its ballistic acceleration upon application of an electric field. From the London equations [6, 7], the acceleration of the supercurrent  $I_s$  and hence  $I$  in the external circuit can be written as [33]·[34]:

$$\frac{dI}{dt} \simeq \frac{dI_s}{dt} = \frac{AV\rho_s}{\mu_0 l} = \frac{V}{L_k}, \quad (3)$$

where  $l$  is the sample length,  $A$  is its cross-sectional area, and  $L_k$  is the kinetic inductance. Kinetic inductive effects become prominent close to  $T_c$  and in ultranarrow interconnects [9, 10]. In our work [11], timescales were chosen to be short enough to have a sufficient magnitude of  $V$  while long enough (compared to characteristic timescales such the gap-relaxation and electron-phonon scattering times) to avoid certain non-equilibrium effects. Variations in fields occur at length scales that are long compared with both  $\lambda$  and the coherence length  $\xi$ , so as to avoid non-local effects. The supercurrent acceleration phase lasts for the duration  $\Delta t \approx j_c \mu_0 \lambda^2 l / V$ , where  $j_c$  demarcates the onset of resistance. Fig. 4(a) and (b) show plots of  $V(t)$  and  $I(t)$  for a Nb sample. The  $I(t)$  function accelerate steadily during the plateau in  $V(t)$ . The ratio  $V(t)/[dI(t)/dt]$  gives the total inductance  $L = L_k + L_g$ , where  $L_g$  is the geometrical inductance. Fig. 4(c) shows the time dependence of  $L(t)$  at various temperatures. Besides the increase in the plateau value of  $L(t)$  with  $T$ , the curves at highest temperatures show  $L(t)$  functions that rise with  $t$  and hence  $I$  (since  $I \propto t$  in this interval as seen in Fig. 4(b)). Since  $\rho_s \propto 1/L_k$ , this is evidence for the suppression of superfluid density through the current's pair-breaking action—a regime not seen before in any other kind of measurement. The fast pulsed signal approach is perhaps unique in its ability to probe the current induced superfluid suppression regime, since continuous-ac probes do not allow high enough excitation levels and tunneling measurements reveal the spectral

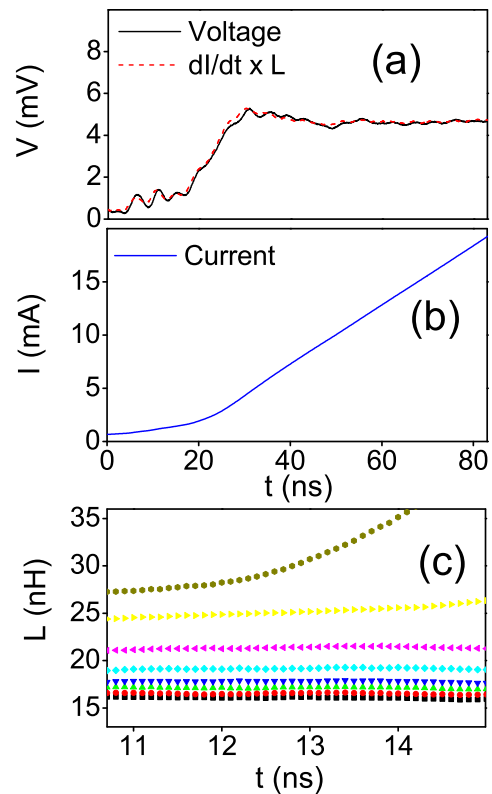


FIG. 4: (a) Applied voltage plateau  $V(t)$  for a Niobium sample. (b) Corresponding  $I(t)$  function rises steadily during the voltage plateau of (a). The corresponding  $dI/dt$  (scaled by a constant  $L$ ) is also plotted on panel (a). (c) Time dependence of measured total inductance,  $L(t) = V(t)/[dI(t)/dt]$  for sample A. The curves are at  $T = 6.10, 5.91, 5.54, 5.17, 4.73, 4.10,$  and  $3.78$  K (from top to bottom). At the highest  $T$ ,  $\rho_s$  ( $\propto 1/L_k$ ) is seen to decline with increasing  $j$  ( $\propto t$ ). (Adapted from G. F. Saracila and M. N. Kunchur, Phys. Rev. Lett. **102**, 077001.)

gap  $\Omega_g$  rather than  $\rho_s$ . This regime is one of the subjects of future study. Interesting dependencies in  $d\rho_s/dj$  can arise in certain situations—for example in the underdoped region of cuprates, where  $j$  may destroy superfluid stiffness without quenching pairing, leaving a pseudogap like state of uncondensed pairs above  $j_d$  [12].

### Current induced pair breaking

Current induced pair breaking provides another window to  $\rho_s$  as well as the normal state at temperatures below  $T_c$ . Unlike the ballistic-acceleration measurements which require much faster time resolutions but are conducted in the dissipationless Meissner regime, a  $j_d$  measurement is difficult because it enters the dissipative regime and, as mentioned in the Background (section ), power densities can get into the GW/cm<sup>3</sup> range. Be-

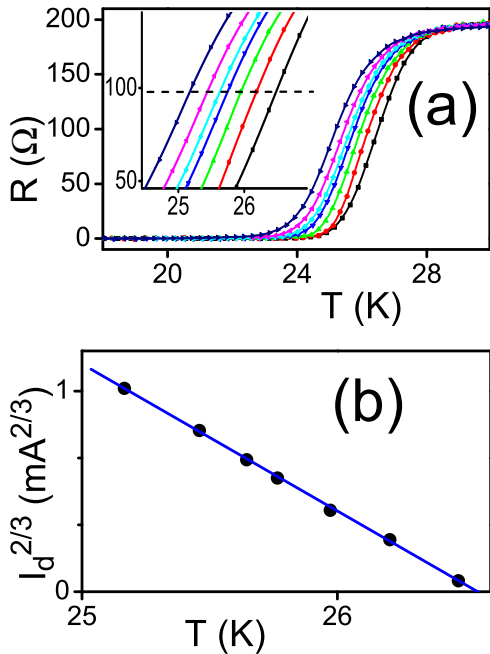


FIG. 5: (a) Resistive transitions measured at various values of constant pulsed current in a  $\text{Sr}_{1-x}\text{La}_x\text{CuO}_2$  film sample. (b)  $I_d^{2/3}$  plotted against the  $T$  values from the inset of panel (a) where the shifted transition curves intersect with the dashed horizontal line. (Adapted from M. Liang, M. N. Kunchur, L. Fruchter, and Z.Z. Li, *Physica C* **492**, 178.)

cause of these technical difficulties,  $j_d$  has been measured in very few superconductors. Our group was the first to measure  $j_d$  in any cuprate superconductor [13] and in  $\text{MgB}_2$  [14], and conducted the most comprehensive test of theories over the entire temperature range [4].

Fig. 5 shows an example of current induced pair breaking close to  $T_c$ , which shows the classic  $j_d^{2/3} \propto [T_c - T]$  behavior in the resistive transition shifts. Fig. 6 shows an example of high pulsed  $IV$  curves, covering the entire temperature range, driving a system into the normal state even at  $T \ll T_c$  (panel c).

As discussed in the Background (section ), a  $j_d$  measurement provides, through Eq. 2, a way to obtain  $\lambda$  and  $\rho_s$  through purely transport measurements that is not directly affected by the material's magnetism. We exploited this fact to obtain  $\rho_s$  in  $\text{Nd}_{2-x}\text{Ce}_x\text{CuO}_4$ , where a large paramagnetic background due to  $\text{Nd}^{3+}$  moments precludes an inductive measurement [15].

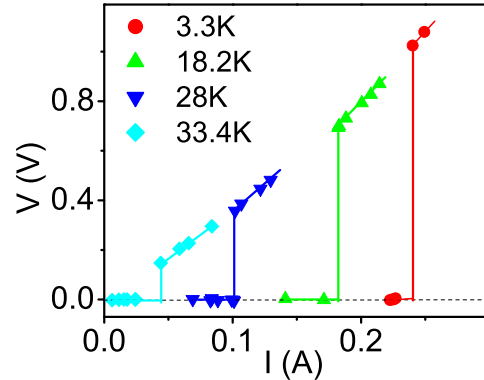


FIG. 6: Current-voltage curves for an  $\text{MgB}_2$  sample at various constant temperatures that drive the system into the normal state even at  $T \ll T_c$ . (Adapted from Topical Review by M. N. Kunchur, *J. Phys.: Condens. Matter* **16**, R1183.)

### Highly driven flux flow

#### *Free flux flow: a window to the normal state*

As soon as an applied magnetic field exceeds  $B_{c1}$ , flux vortices penetrate the sample. The Lorentz force of a transport current will then potentially induce flux motion and consequently resistance. Numerous regimes of flux dynamics exist ([3]) but the simplest is the regime of free flux flow when the pinning force is negligible compared to the Lorentz force. However, as explained in the Background (section ), the requirement of high driving forces and accompanying dissipation make this FFF regime also very illusive. FFF was quantitatively confirmed for the first time in any superconductor by our group in a  $\text{Y}_1\text{Ba}_2\text{Cu}_3\text{O}_7$  film [16] (this result is cited in Tinkham's textbook [7]). As explained earlier, the vortex core provides another window to the normal state (which is more easily accessible than destroying the superconductivity with pair-breaking currents). As shown in Fig. 7, this concept was fruitfully used [17] to elucidate  $\rho_n(T)$  over the entire range for  $\text{Y}_1\text{Ba}_2\text{Cu}_3\text{O}_7$  and to prove that it had a metallic normal state, i.e.,  $\rho_n \rightarrow \text{const}$  as  $T \rightarrow 0$ .

In other work, combining the extremely low pinning in MoGe alloy films with our high driving forces so that pinning was essentially absent, we were able to sensitively and quantitatively assess the nature of flux dynamics [18] beyond the Bardeen-Stephen approximation. In particular, we were able to differentiate between the TDGL (time dependent Ginzburg-Landau) theory [19, 20] and the microscopic LO (Larkin-Ovchinnikov) theory [21]. As shown in Fig. 8, we found that the mean-field result arising out of TDGL provides a much better description of FFF than the theory of Larkin and Ovchinnikov; these

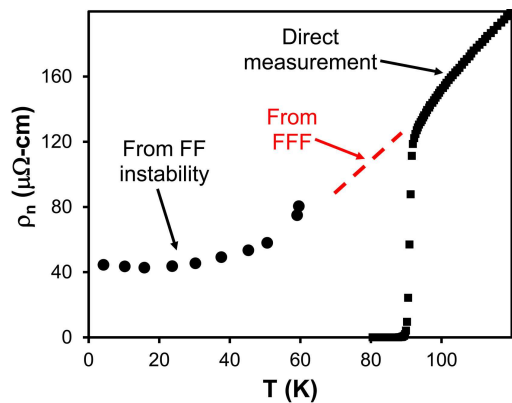


FIG. 7: The vortex core as a window to the normal state: Free flux flow and the flux-flow instability together elucidate the normal-state resistivity  $\rho_n(T)$  in  $Y_1Ba_2Cu_3O_7$  over the entire temperature range. The measurements indicate a metallic normal state, i.e.,  $\rho_n \rightarrow \text{const}$  as  $T \rightarrow 0$ . (Adapted from M. N. Kunchur, D. K. Christen, and J. M. Phillips, Phys. Rev. Lett. 70, 998; and M. N. Kunchur, B. I. Ivlev, D. K. Christen, and J. M. Phillips, Phys. Rev. Lett. 84, 5204.)

results represent to most complete tests of the fundamental flux-flow theories [18].

#### Flux-flow instability and the spectral function

At high levels of  $j$  and  $E$ , the quasiparticle distribution function departs sufficiently from equilibrium so as to alter the vortex dynamics. If  $\rho_f$  rises with  $j$  sufficiently rapidly,  $j(E)$  turns over and exhibits a negative differential conductivity as shown in Fig. 9(a). In a current biased measurement this leads to a flux-flow instability ( $E$  jumps above a critical value  $E^*$ ). Two principal scenarios are possible. One occurs when the average energy increase is not significant but the distribution function acquires a non-thermal shape—the Larkin-Ovchinnikov (LO) instability [22] which occurs close to  $T_c$  and when  $\tau_{ee} \gg \tau_{ep}$ . The other kind is the hot-electron instability, first established by our group [23, 24], which results when the electron temperature rises while maintaining a thermal like distribution function shape; this instability is more likely at temperatures well below  $T_c$  and when  $\tau_{ee} \ll \tau_{ep}$ . Flux-flow instabilities have been experimentally investigated for some time (e.g., Refs. [25]–[26]) but before our group established the hot-electron instability, experimental results have been analyzed, sometimes incorrectly, almost entirely in terms of the LO effect. Recent works have now begun to interpret their findings using our hot-electron picture. In the course of investigating the hot-electron instability, we discovered new secondary effects (Fig. 9(b)) related to the fragmentation of the moving flux into elastic domains, that lead to Gunn-effect like steps in the  $IV$  curve [27, 28]. Fig. 9

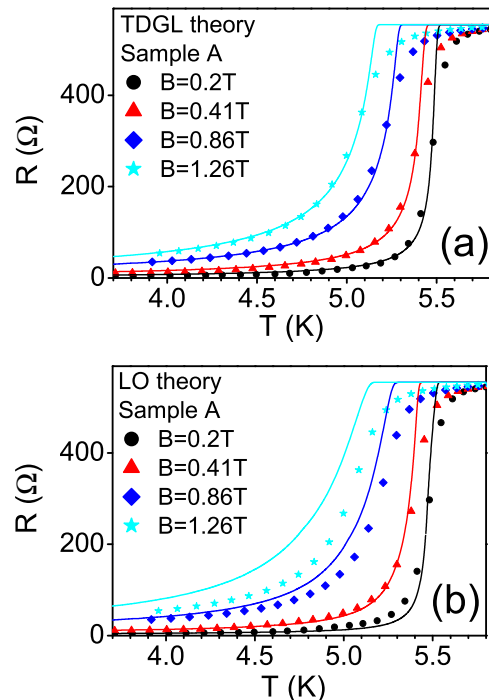


FIG. 8: Detailed tests of the ideal free-flux-flow response beyond the Bardeen-Stephen approximation, comparing the TDGL and LO theories. These experiments provided the first quantitative validation of the TDGL (time dependent Ginzburg-Landau) theory for the FFF response. (Adapted from M. Liang, M. N. Kunchur, J. Hua and Z. Xiao, Phys. Rev. B 82, 064502.)

shows our various results related to the hot-electron instability. Ref. [29] gives a general overview on the subject of non-monotonic responses and instabilities.

These flux-flow instabilities serve as tools that yield valuable information on the energy relaxation time  $\tau_e$  between quasiparticles and lattice, which in turn sheds light on  $\alpha^2 F$  the electron-phonon spectral function[35]. It can be shown [24] that  $jE \simeq (P_e + P_r)$  in the steady state, where the powers  $P_e$  and  $P_r$  correspond to the two lowest order processes of phonon emission and quasiparticle recombination respectively. Each of  $P_e$  and  $P_r$  can be calculated in terms of  $\alpha^2 F$ ; for example,  $P_e$  has the form[36]

$$P_e = \frac{2Vm^2}{\pi\hbar^3} \int \int \int d\omega d\epsilon d\epsilon' v_F \alpha^2(\omega) F(\omega) \hbar\omega f_e(E, E') \delta(E - E' - \hbar\omega) \quad (4)$$

Thus the hot-electron instability gives a weighted average of  $\alpha^2 F$  that involves purely the processes that transfer energy between quasiparticles and phonons. Hence this provides a different window to this important quantity compared to some of the traditional techniques such as tunneling, ARPES, optical conductivity, and neutron

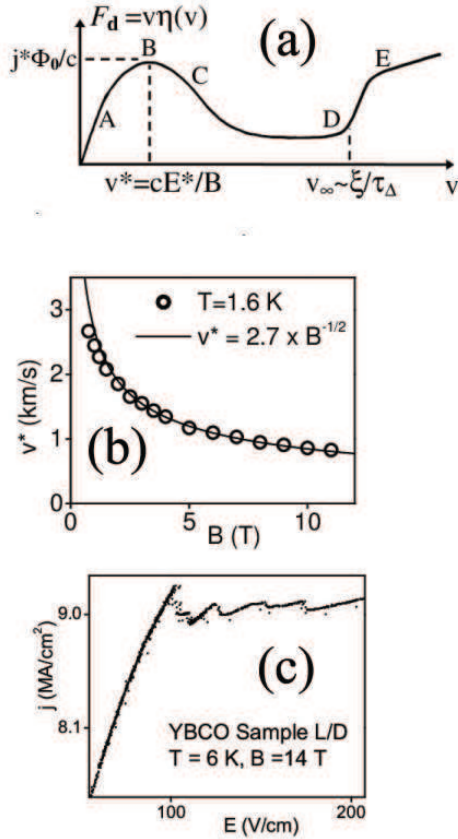


FIG. 9: (a) The primitive curve for the hot-electron regime (b) The measured critical vortex velocity  $v^*(B)$  (corresponding to point B on the primitive curve) shows the predicted  $1/\sqrt{B}$  dependence. (c) Shear distortions cause a sawtooth shaped  $IV$  curve beyond the instability. (Adapted from M. N. Kunchur, B.I. Ivlev, and J. M. Knight, Phys. Rev. Lett. **87**, 177001; M. N. Kunchur, Phys. Rev. Lett. **89**, 137005; M. N. Kunchur, B.I. Ivlev, and J. M. Knight, Phys. Rev. B **66**, 60505.)

scattering. These other techniques also sense coupling between electrons and other types of excitations besides just phonons (e.g., optical conductivity also includes the contribution of spin fluctuations to the inelastic electronic scattering [30, 31]).

### CONCLUDING REMARKS

The fast-timescale and high-dissipation techniques that our group has developed over the past twenty five years provide some unique windows to fundamental parameters and various physical phenomena and regimes in superconductors.

Besides the basic-science importance, these types of measurements also have implications for applications, since the experiments chart the detailed growth  $E(j)$  as the current density  $j$  is varied from the onset of dissipa-

tion at  $j_c$ , to the complete destruction of superconductivity at the depairing value  $j_d$ . Knowledge of this  $E(j)$  function is especially important for applications that operate dissipatively above  $j_c$  for short durations (such as pulsed superconducting magnets that might be used for fusion-energy research) but also for applications that operate in the dissipationless mode ( $j < j_c$ ) to optimize the normally conducting encapsulations of superconductive tapes and wires [32]. The fast time-scale studies related to kinetic inductance and superfluid suppression are relevant for devices such as superconducting photon detectors.

Thus we believe that our collaborations with groups developing the latest materials, in the quest for room-temperature superconductor, will lead to fruitful results.

### ACKNOWLEDGEMENTS

We would like to acknowledge D. K. Christen, C. E. Klabunde, J. M. Phillips, D. H. Arcos, C. Wu, G. F. Saracila, M. Liang, N. Shayesteh-Moghadam, S. D. Varner, J. M. Knight, B. Ivlev, S. Mejia-Rosales, A. Gurevich, E.-M. Choi, K. H.P. Kim, W. N. Kang, and S.-I. Lee, Y. Cui, A. Pogrebnyakov, P. Orgiani, X. X. Xi, P. W. Adams, D. P. Young, J. Hua, Z. Xiao, A. Guarino, A. Leo, G. Grimaldi, N. Martucciello, C. Dean, M. N. Kunchur, S. Pace, A. Nigro, L. Fruchter, Z.Z. Li, Q.L. He, H. Liu, J. Wang, R. Lortz, and I.K. Sou. This work was supported by the U. S. Department of Energy, Office of Science, Office of Basic Energy Sciences, under grant number DE-FG02-99ER45763.

\* Corresponding author email: kunchur@sc.edu; URL: <http://www.physics.sc.edu/~kunchur>

- [1] A. P. Drozdov, M. I. Erements, I. A. Troyan, V. Ksenofontov, and S. I. Shylin, *Conventional superconductivity at 203 kelvin at high pressures in the sulfur hydride system*, Nature 525, 73 (2015).
- [2] C. E. Precker, P. D. Esquinazi, A. Champi, J. Barzola-Quiquia, M. Zoraghi, S. Muinos-Landin, A. Setzer, W. Bohlmann, D. Spemann, J. Meijer, T. Muenster, O. Baehre, G. Kloess, and H. Beth, *Identification of a possible superconducting transition above room temperature in natural graphite crystals*, New J. Phys. 18, 113041 (2016).
- [3] G. Blatter, M. V. Feigel'man, V. B. Mikhail, A. I. Larkin, and V. M. Valerii, *Vortices in high-temperature superconductors*, Rev. Mod. Phys. 66, 1125 (1994).
- [4] M. N. Kunchur, *Current induced pair breaking in Magnesium Diboride*, Topical Review in J. Phys.: Cond. Matter 16, R1183-R1204 (2004).
- [5] M. N. Kunchur, *Novel transport behavior found in the dissipative regime of superconductors*, Mod. Phys. Lett. B. 9, 399 (1995).

- [6] F. London, and H. London, *The electromagnetic equations of the superconductor*, Proc. R. Soc. A 149, 71 (1935).
- [7] Michael Tinkham, *Introduction to Superconductivity*, 2nd Edition, McGraw Hill, New York (1996).
- [8] P. D. Scholten, J. D. Lejeune, W. M. Saslow, and D. G. Naugle, *Low-frequency electromagnetic response function for strong-coupling superconductors*, Phys. Rev. B. 16, 1068 (1977).
- [9] I. F. Oppenheim, S. Frota-Pessoa, and M. Octavio, *Time delay in the response of superconducting filaments to supercritical current pulses*, Phys. Rev. B. 25, 4495 (1982).
- [10] J. Y. Y. Lee and T. R. Lemberger, *Penetration depth  $\lambda(T)$  of  $YBa_2Cu_3O_7$  films determined from the kinetic inductance*, Appl. Phys. Lett. 62, 2419 (1993).
- [11] G. F. Saracila and M. N. Kunchur, *Ballistic acceleration of a supercurrent in a superconductor*, Phys. Rev. Lett. 102, 077001 (Feb. 20, 2009).
- [12] L. Goren, and E. Altmun, *Quenching the superconducting state of cuprate compounds with electric currents: A variational study*, Phys. Rev. Lett. 104, 257002 (2010).
- [13] M. N. Kunchur, D. K. Christen, C. E. Klabunde, and J. M. Phillips, *Pair-breaking effect of high current densities on the superconducting transition on  $YBa_2Cu_3O_7$* , Phys. Rev. Lett. 72, 752 (1994).
- [14] M. N. Kunchur, Sung-Ik Lee, and W. N. Kang, *The pair-breaking critical current density of magnesium diboride*, Phys. Rev. B. 68, 064516 (2003).
- [15] M. N. Kunchur, C. Dean, M. Liang, N. S. Moghaddam, A. Guarino, A. Nigro, G. Grimaldi, A. Leo, *Depairing current density of  $Nd_{2-x}Ce_xCuO_{4-d}$  superconducting films*, Physica C 495, 66 (2013).
- [16] M. N. Kunchur, D. K. Christen, and J. M. Phillips, *Observation of free flux flow at high dissipation levels in  $YBa_2Cu_3O_7$  epitaxial films*, Phys. Rev. Lett. 70, 998 (1993).
- [17] M. N. Kunchur, B. I. Ivlev, D. K. Christen, and J. M. Phillips, *Metallic normal state of  $YBa_2Cu_3O_7$* , Phys. Rev. Lett. 84, 5204 (2000).
- [18] M. Liang, M. N. Kunchur, J. Hua and Z. Xiao, *Evaluating free flux flow in low-pinning molybdenum-germanium superconducting films*, Phys. Rev. B 82, 064502 (2010).
- [19] S. Ullah and A. T. Dorsey, *Effect of fluctuations on the transport properties of type-II superconductors in a magnetic field*, Phys. Rev. B. 44, 262 (1991).
- [20] A. T. Dorsey, *Vortex motion and the Hall effect in type-II superconductors: A time-dependent Ginzburg-Landau theory approach*, Phys. Rev. B. 46, 8376 (1992).
- [21] A. I. Larkin and Yu. N. Ovchinnikov, in *Nonequilibrium Superconductivity*, edited by D. N. Langenberg and A. I. Larkin (Elsevier, Amsterdam, 1986), Chap. 11.
- [22] A. I. Larkin and Yu. N. Ovchinnikov, *Nonlinear conductivity of superconductors in the mixed state*, Zh. Eksp. Teor. Fiz. 68, 1915 (1975) [Sov. Phys. JETP 41, 960 (1976)].
- [23] M. N. Kunchur, *Unstable flux flow due to heated electrons in superconducting films*, Phys. Rev. Lett. 89, 137005 (2002).
- [24] J.M. Knight and M. N. Kunchur, *Energy relaxation at a hot-electron vortex instability*, Phys. Rev. B 74, 64512 (2006).
- [25] L. E. Musienko, I. M. Dmitrenko, and V. G. Volotskaya, *Nonlinear conductivity of thin films in the mixed state*, Pis'ma Zh. Eksp. Teor. Fiz. 31, 603 (1980) [JETP Lett. 31, 567 (1980)].
- [26] G. Grimaldi, A. Leo, A. Nigro, S. Pace, and R. P. Huebener, *Dynamic ordering and instability of the vortex lattice in Nb films exhibiting moderately strong pinning*, Phys. Rev. B. 80, 144521 (2009).
- [27] M. N. Kunchur, B.I. Ivlev, and J. M. Knight, *Steps in the negative-differential-conductivity regime of a superconductor*, Phys. Rev. Lett. 87, 177001 (2001).
- [28] M. N. Kunchur, B.I. Ivlev, and J. M. Knight, *Shear fragmentation of unstable flux flow*, Phys. Rev. B 66, 060505 (2002).
- [29] V. R. Misko, S. Savel'ev, Alexander L. Rakhmanov, and Franco Nori, *Negative differential resistivity in superconductors with periodic arrays of pinning sites*, Phys. Rev. B 75, 024509 (2007).
- [30] J. P. Carbotte, E. Schachlinger, and D. N. Basov, *Coupling strength of charge carriers to spin fluctuations in high-temperature superconductors*, Nature 401, 354 (1999).
- [31] J. J. Tu, C. C. Homes, G. D. Gu, D. N. Basov, and M. Strongin, *Optical studies of charge dynamics in optimally doped  $Bi_2Sr_2CaCu_2O_8$* , Phys. Rev. B. 66, 144514 (2002).
- [32] M. N. Kunchur, D. K. Christen, C. E. Klabunde, and K. Salama, *Exploring the dissipative regime of superconductors for practical current-lead applications*, Appl. Phys. Lett. 67, 848 (1995).
- [33] In more detail [8],  $L_k \propto I(0,0,T)$ , where the superconductor's electromagnetic response function  $I(\omega, \vec{R}, T)$  is defined by  $\vec{j}(\vec{r}, \omega) = \frac{e^2 N(0) v_F}{2\pi^2 \hbar c} \times \int \frac{\vec{R}[\vec{R} \cdot \vec{A}_\omega(\vec{r}')] }{R^4} I(\omega, \vec{R}, T) d\vec{r}'$ , and  $I(\omega, \vec{R}, T)$  is related to the electron-phonon spectral function  $\alpha^2(\omega)F(\omega)$ .
- [34] The normal-current component  $j_n \approx (n_n/n)\sigma_n E$ , which results from the electric field present during superfluid acceleration, is several orders of magnitude smaller than  $j_s$  at the frequencies of the experiment.
- [35] This spectral function is defined as  $\alpha^2 F = \frac{V}{(2\pi)^3 \hbar^2} \int \frac{d^2 k'}{v_F} |\mathcal{M}_{k=k'}|^2 \delta(\omega - c_s |k - k'|)$ , where  $\mathcal{M}_{k=k'}$  is the electron-phonon matrix element.
- [36] Here  $f_e(E, E') = \frac{f(E_k)[1-f(E'_k)]}{1-f(E_k)} \left(1 - \frac{\Delta_k \Delta_{k'}}{E_k E_{k'}}\right)$  combines the coherence and occupation factors.